PROCEEDINGS, 51st Workshop on Geothermal Reservoir Engineering
Stanford University, Stanford, California, February 9-11, 2026
SGP-TR-230

Identification of Fracture Flow Pathways at Utah FORGE Following Stimulation Activities in 2022 and 2024

Aleta Finnila

WSP, Redmond, WA

aleta.finnila@wsp.com

Keywords: FORGE, DFN, fracture model, EGS

ABSTRACT

A comprehensive update to the Reference Discrete Fracture Network (DFN) model for the Frontier Observatory for Research in Geothermal Energy (FORGE) site near Milford, Utah, has been completed. This revision was informed by the identification of flow pathways between wells 16A(78)-32 and 16B(78)-32 following stimulation activities conducted in 2022 and 2024. Designated as the Utah FORGE 2025 v1 DFN, the revised model includes 131 discrete planar fractures with radius values ranging from 14 to 780 m and 19,544 stochastic fractures located away from well control with radius values ranging from 20 to 149 m. Discrete fractures in the DFN were identified using updated microearthquake data from surface arrays and deep geophones, fracture interpretations from FMI and UBI logs (with aperture estimates when available), k-means cluster rock type analysis from various well logs, frac hit data, and core samples. This paper describes the methodology used for mapping fracture pathways in the reservoir. While fracture geometry is detailed in the revised DFN model, hydraulic properties are not assigned. Notably, natural fractures primarily account for the observed stimulated flow in this model, with just a few induced hydraulic fractures added to connect the natural fracture pathways to some well casing perforation intervals.

1. INTRODUCTION

Development of the current Utah FORGE DFN model was motivated by the need of the wider FORGE modeling community to simulate circulation between wells 16A(78)-32 and 16B(78)-32. These simulations are used to predict both thermal and tracer breakthrough times for future circulation tests. As such, the fracture model includes fractures active in post-stimulation flow pathways, so both pre-existing natural fractures and new induced tensile fractures are included. Modelers wishing to simulate earlier stimulation events may wish to remove the hydraulic fractures from the full set provided in the Geothermal Data Repository (GDR). This DFN release is referred to as the Utah FORGE 2025 v1 DFN release (DFN). The GDR release of the DFN includes fracture files, well trajectories, and region boxes in both global coordinates with Imperial units and a rotated, local coordinate frame aligned with the principal stress directions in SI units (Finnila, 2025).

Since the last major fracture model released in 2024 (see Finnila and Jones, 2024a), well 16A(78)-32 has had further stimulation work and well 16B(78)-32 has also been stimulated. Analysis of microseismic events triggered during the stimulation activities has resulted in the release of micro-earthquake (MEQ) catalogs showing both locations and magnitudes of these events. Linear and planar patterns present in the microseismic point clouds offer strong evidence of flow pathways extending to regions far from the injection intervals in well 16A(78)-32. However, the absence of seismicity does not eliminate the possibility of flow, as aseismic stimulation is also likely taking place within the FORGE reservoir. Some spinner log data is available to show where flow is initiating in the reservoir from well 16A(78)-32 and entering well 16B(78)-32, although this data set is not comprehensive in coverage along all the well perforated or open sections or consistent between circulation tests. The best evidence for where flow pathways intersect well 16B(78)-32 currently comes from the Fracture Driven Interactions (FDIs or frac hits) recorded by the fiber optics that had been cemented behind the well casing. Minor DFN updates based on the newly acquired MEQ catalogs were released to the GDR in 2024 (Finnila and Jones, 2024b). These MEQ catalogs have subsequently been updated with the new point locations seeming to align more consistently with the other data sets based on the current DFN development work.

While early FORGE fracture models starting in 2019 were primarily stochastic in nature, this current version is dominated by discrete features. Increasing numbers of deep wells with extensive logging as well as stimulation activities are now providing rich data sets that provide evidence for individual, significant features that can now be included in the fracture models. This paper first describes the DFN and then includes an example of the development workflow using two of the discrete fractures included in the model. This is followed by figures showing correlations between the DFN fractures and some of the input data sets. The concluding section lists some of the current DFN limitations and includes observations made during the development process.

2. DFN DESCRIPTION

To meet the requirements of modelers wanting to simulate flow between 16A(78)-32 and 16B(78)-32 during circulation testing, the DFN needed to meet the following main expectations. It should:

- form a connected fracture network between open hole and perforated casing intervals on well 16A(78)-32 and open hole and perforated casing intervals on well 16B(78)-32

- include fractures that align with planar microseismic point locations that were recorded during stimulation activities
- include fractures that intersect with well 16B(78)-32 at frac hit locations

There seems to be sufficient data available at Utah FORGE now to identify enough discrete fractures to satisfy these requirements. Additionally, stochastic fractures are provided as in previous DFN versions for model regions lacking specific data. The discrete fractures and stochastic fractures are provided in the GDR release in separate files so they can be used independently if desired.

2.1 Discrete fractures

The DFN includes 131 discrete fractures. Two of the fractures are provided with two different fracture sizes, so the total number of fractures is sometimes referred to as 133. These fractures are shown in Figure 1. The discrete fractures are larger than in previous DFN versions due to the recent availability of more MEQ catalogs which allow for extension of features over longer distances, as well as the new analysis done for this work to correlate features across wells. Thousands of figures were generated to document the correlation of each fracture with the available data sets. These figures are compiled in a new GDR release and organized by both fracture and data set Finnila, 2026).

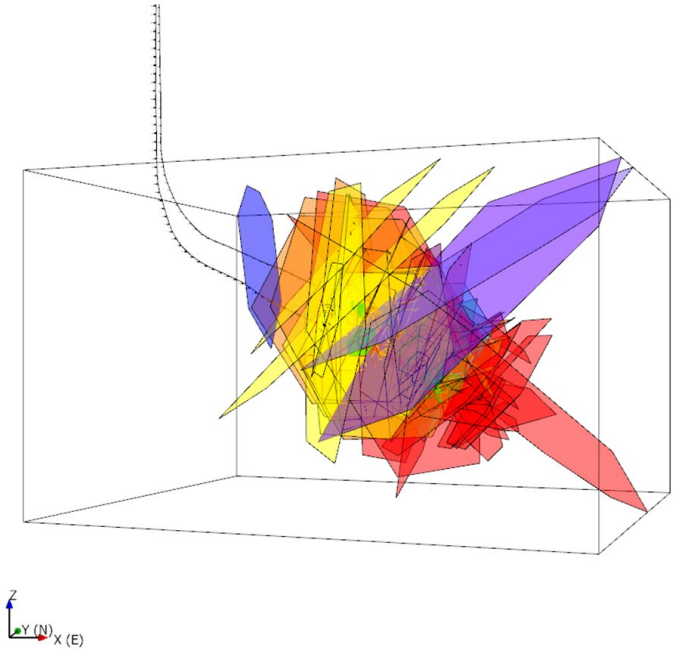

Figure 1: The 131 discrete fractures included in the Utah FORGE 2025 v1 DFN. Colors of fractures indicate identification order with respect to well 16A(78)-32 stimulation stage (Finnila, 2025).

The discrete fractures have been individually described using a complex naming convention with the intention that modelers may pick and choose a customized subset to include for any particular modeling task (Figure 2).

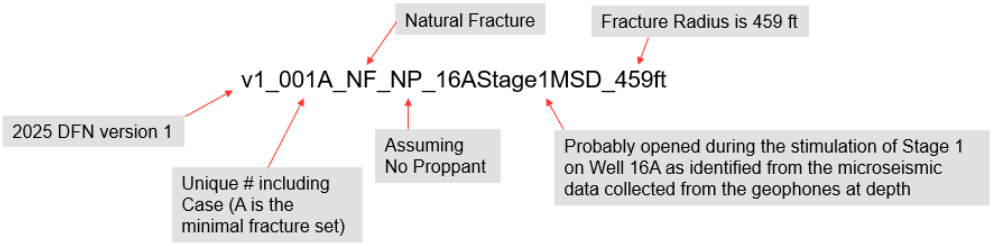

Figure 2: Example showing parts of the DFN discrete fracture naming convention.

Fracture identifiers include the following naming conventions:

- DFN Version: All the fractures in the 2025 DFN version 1 have names starting with “v1”.

- Numeric Identifier: Three-digit number that is unique for the location and orientation of the fracture (but not size). The combination of the numeric identifier and the Case will be unique. The numbering generally reflects the order in which the fracture locations were revealed from timing of the microseismic data, so fractures associated with the 16A(78)-32 Stage 1 stimulation have the smallest numbers.
- Case Options:
    - A: Minimal fracture set required to connect 16A(78)-32 with 16B(78)-32
    - B: Additional fractures (in addition to Case A) required to match observed microseismic data, significant features from well log data, and frac hits on 16B(78)-32
    - S: Significant, large-scale structural fractures that may or may not be involved in current stimulated flow paths and may be larger versions of either Case A or Case B fractures
- Fracture Type (assumed):
    - NF: Natural Fracture
    - HF: Hydraulic Fracture
- Proppant (assumed):
    - PP: Presumed to be filled with proppant (intersecting or close to a stimulation stage that used proppant). Stages with pumped proppant include 16A(78)-32 Stages 3R, 4, 5, 8, 9, 10 and 16B(78)-32 Stages 1, 2, 3, 4.
    - NP: Assumed to have no proppant
- Primary Evidence Source: Stimulation stage where fractures were identified (primarily) from microseismic activity – currently 16A(78)-32 Stages 1 – 10. This is followed by a data type source:
    - FH: Included primarily to reach a frac hit location on 16B(78)-32
    - FMI16A: Identified from the Schlumberger fracture interpretation of 16A(78)-32 FMI
    - FMI16AH: Identified from the Handwerger fracture interpretation of 16A(78)-32 FMI
    - FMI16B: Identified from the Schlumberger fracture interpretation of 16B(78)-32 FMI
    - HF: Added as a new hydraulic fracture (generally only done if there is no evidence of a natural fracture)
    - MSD: Location, size, and orientation selected based on microseismic data collected at depth
    - MSS: Location, size, and orientation selected based on microseismic data collected at the surface
    - MSDS: Combination of both MSD and MSS
    - PF: Included primarily to intersect a well at a perforation interval
    - UBI16B: Identified from the Schlumberger fracture interpretation of 16B(78)-32 UBI
- Fracture Radius: Circular fractures are assumed for modeling convenience. The radius is included in the name for easy sorting of larger and smaller fractures. This may be useful for assigning fracture apertures and permeability/transmissivity as larger fractures tend to have larger hydraulic apertures. The largest features may also reveal lithology boundaries or fault zones.

2.2 Stochastic fractures

Stochastic fractures in the DFN are randomly generated based on underlying parameterized distributions for fracture sizes and orientations with fracture intensity or density fixed at a set value for the overall region. These constraints were not changed from the 2024 DFN but a new realization was generated for the 2025 v1 DFN which is shown in Figure 3. The fractures were first generated throughout the entire modeling region and then fractures that intersected the wells 16A(78)-32 or 16B(78)-32 were removed as this near-wellbore region is effectively populated by the discrete fracture set.

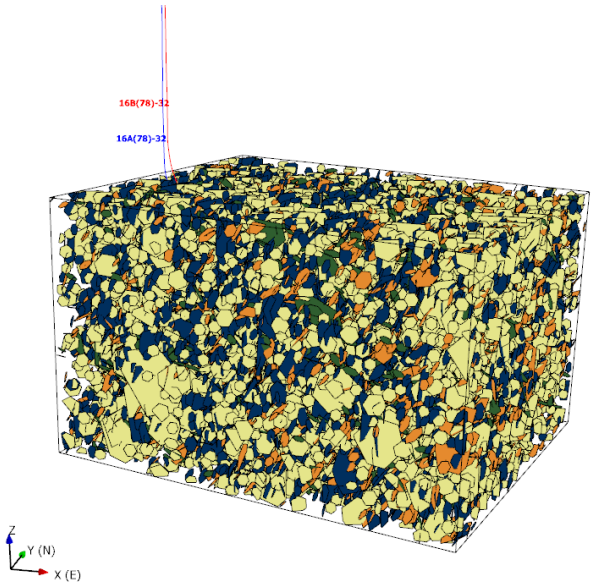

Figure 3: Stochastic fractures included in the Utah FORGE 2025 v1 DFN (Finnila, 2025).

For convenience, the 2024 parameterization of the stochastic fractures is repeated in this paper, see Finnila and Jones (2024a) for details. Table 1 shows the Fisher distribution parameters of the four orientation sets included in the full stochastic fracture set.

Table 1. Stochastic fracture set orientations.

Set Name	Description	Trend/Plunge (deg)	Strike/Dip (deg)	Fisher Concentration	%
Set 1	East-striking, sub-vertical dipping South	358/12	88/78	20	35
Set 2	SSW-striking, vertical	115/3	205/87	15	35
Set 3	South-striking moderately dipping West	75/35	165/55	10	20
Set 4	North-striking, moderately dipping East	230/50	320/40	7	10

Stochastic fracture sizes were generated using a truncated power law distribution having a power law exponent of 3.2 and a minimum fracture radius of 0.63 m. Generated stochastic fracture sizes in the DFN are between 20 m and 150 m for the equivalent radius (R_e) of the fracture. The R_e of a fracture is defined as the radius of a circle having the same fracture area as the actual fracture (which may not be circular). Fractures are assumed to have roughly circular shapes and are included in the DFN as planar regular hexagons.

The fracture intensity of the stochastic fractures is described by the total fracture area dived by the region volume (P_{32}). When generating the stochastic fracture sets in the reference DFN, the target intensity is adjusted based on the truncated size population generated. For the set of fractures generated having an equivalent radius between 20 m and 150 m, the target P_{32} values in the modeling region was 0.0196 1/m.

2.3 Comparison between discrete and stochastic fractures

Figure 4 shows contour stereonets showing the orientations of both the stochastic fractures and the discrete fractures included in the DFN. It is striking how similar the contour plots are for the two fracture categories. While the SSW-striking, vertical Fisher set is more prominent in the discrete fractures and the East-striking, sob-vertical dipping South set is more prominent in the stochastic fractures, the same four sets are present.

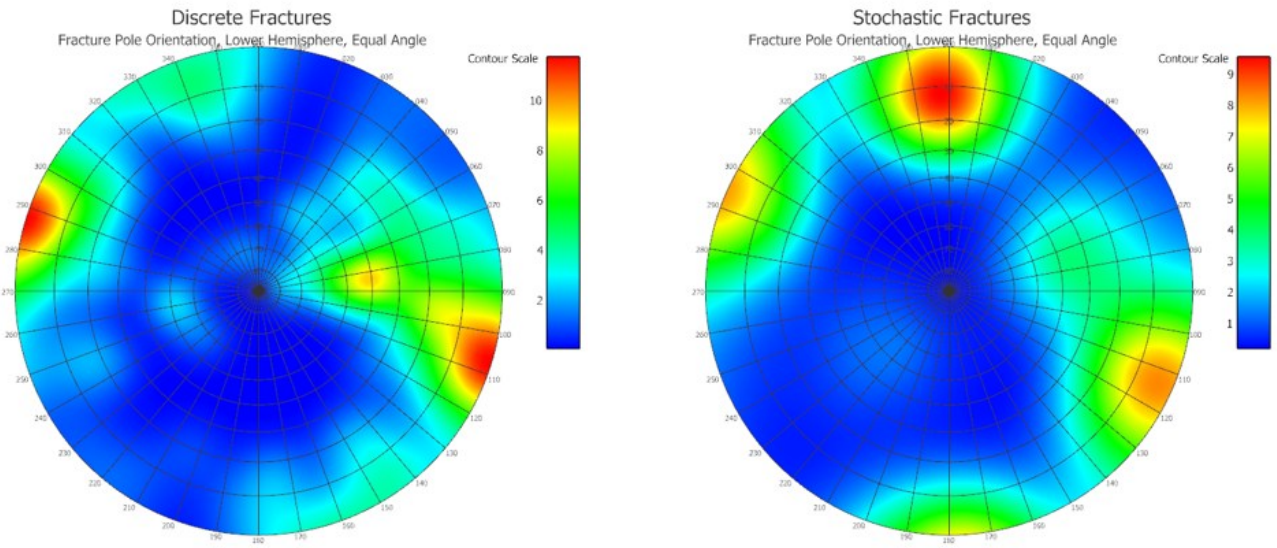

Figure 4: Contour stereonet plots showing orientations of the discrete and stochastic fractures included in the DFN.

3. DFN DEVELOPMENT PROCESS

The DFN development workflow can be described in the following steps. For each stimulation stage in well 16A(78)-32:

- Start at well 16A(78)-32 perforation interval or open hole section. Is there any spinner log data to suggest this interval is active in a flow pathway?
- If so (or if no spinner log data available), look for potential natural fractures intersecting this interval in the interpreted FMI log.
- Check for any early time microseismic activity that might show active fractures near the perforations/open hole.
- If no natural fractures are good candidates, add a new hydraulic fracture to connect with the perforation interval.
- Connect fractures that are intersecting the perforation/open intervals with any fractures fit to microseismic point data lying between wells 16A(78)-32 and 16B(78)-32.

- For any fracture identified primarily from microseismic data that intersects the wells, check all available log data sources for evidence of a fracture at this location (e.g. FMI, UBI, sonic, spectral, and k-means cluster analysis results).
- Check for connections between these emerging flow pathways and any frac hit locations recorded on well 16B(78)-32.
- For any frac hit locations on well 16B(78)-32 that are not already connected to a flow pathway, check for any natural fractures that intersect these locations. If present, extend them to reach one of the flow pathways. If no pre-existing natural fractures are located near the frac hit locations, create a new hydraulic fracture to make the connection.
- Add fractures away from well control that seem to be indicated by microseismic data and make sure they are connected to the growing DFN.

After developing the DFN fractures stage by stage, check for any other significant fractures that may be present:

- Check for significant natural fractures intersecting the three vertical deep wells (58-32, 56-32, 78B-32) and if there is microseismic data to support their being active during the stimulation of wells 16A(78)-32 or 16B(78)-32, add these to the DFN and make sure they are connected to the growing DFN.
- Add any other fractures that have significant data support even if they do not seem to be active during the stimulation activities of wells 16A(78)-32 or 16B(78)-32 (these do not need to be connected to the fractures indicated in flow activity).

As an example of this workflow, two fractures developed for well 16A(78)-32 stimulation Stage 3 are shown. Stage 3 has a lot of data including MEQ catalogs from both the original stimulation activity for well 16A(78)-32 in 2022 that did not include proppant and the Stage 3R re-frac that occurred in 2024 which did include proppant. An early assumption regarding the flow pathway between the perforation interval on well 16A(78)-32 and the sizable frac hit location on 16B(78)-32 directly above this location was that a single, new hydraulic fracture was connecting the two wells (Figure 5). The current analysis described below suggests that two connected, steeply-dipping, pre-existing natural fractures are more consistent with the available data. However, since the resulting flow pathway between these two interpretations is not significantly different in terms of the total fracture area or shortest path between the two wells, simulations using either of these fracture models (single hydraulic fracture vs two natural fractures) would probably show similar results for this particular stage. The following detailed description of the workflow used to define the two natural fractures is done in to illustrate the methodology, not to discredit previous work on modeling this stage using simulations based on a single hydraulic fracture.

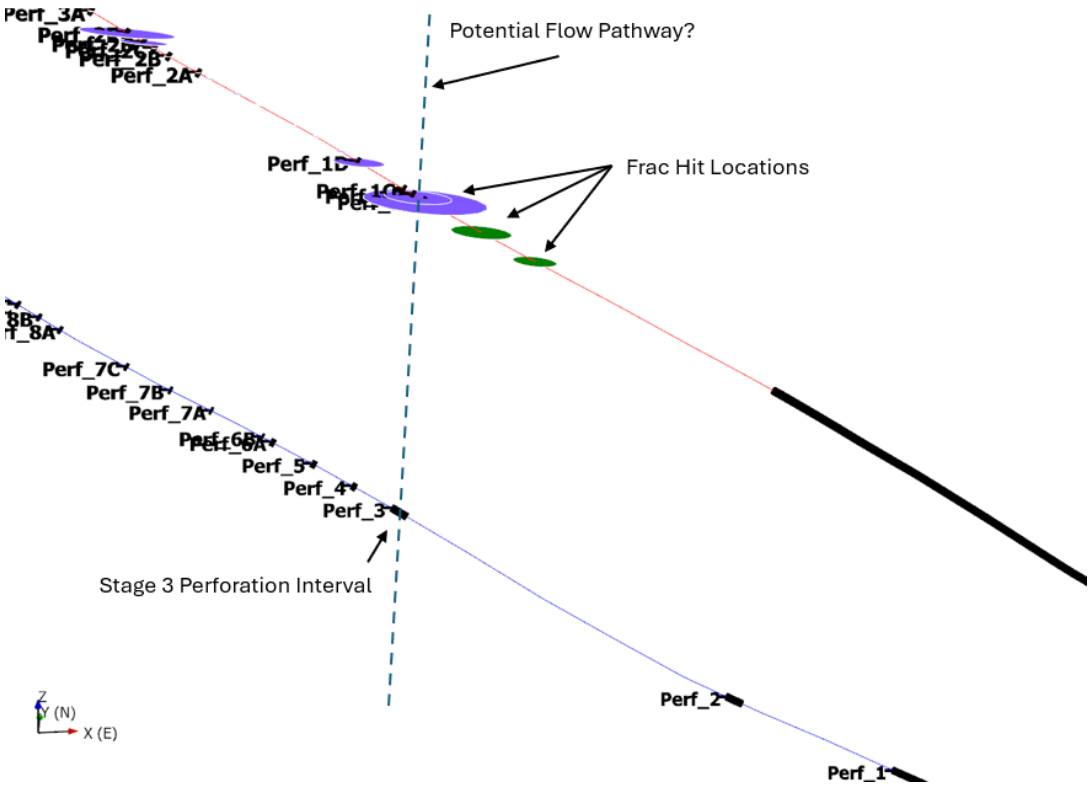

Figure 5: Starting workflow to find fractures for flow pathway created during stimulation of Stage 3 in well 16A(78)-32.

Stimulation of well 16A(78)-32 in 2022 produced a swarm of microseismic activity that was captured using geophones installed at depth in the surrounding deep vertical monitoring wells. The locations of these events were first published in MEQ catalogs in 2022 and subsequently revised in 2023 (Dyer et al, 2023). Figure 6 shows the revised point locations which occur in a wedge-shaped volume as viewed from the south.

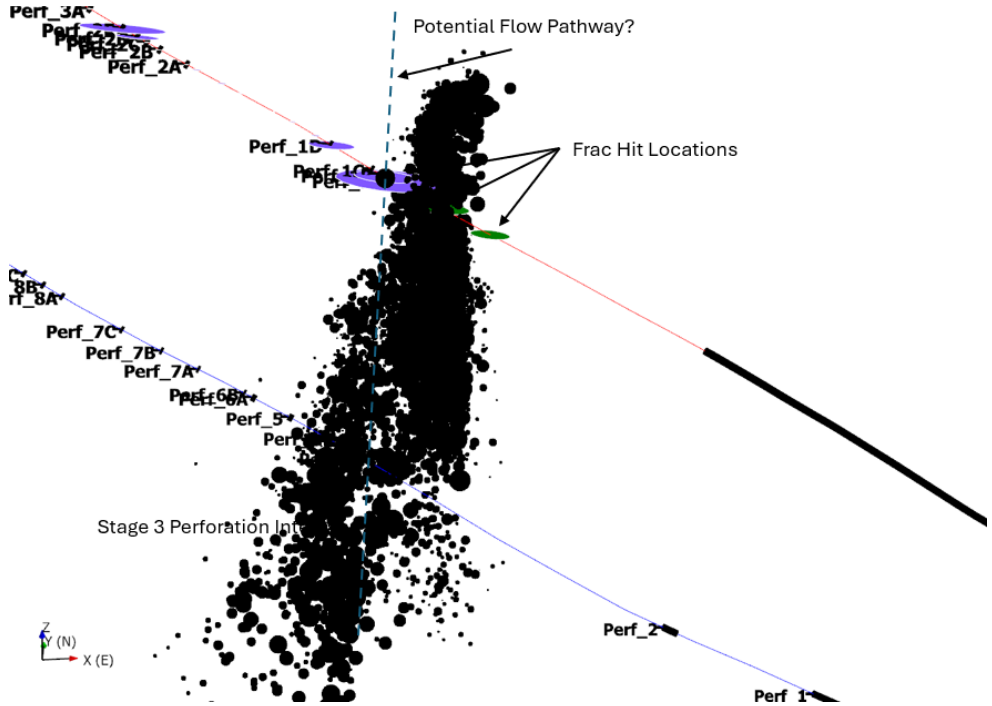

Figure 6: Microseismic point cloud recorded during the 2022 stimulation of Stage 3 in well 16A(78)-32 (MEQ data from Dyer et al, 2023).

Figure 7 shows microseismic locations recorded in just the first 30 minutes of the Stage 3 stimulation with MEQ points colored by elapsed time and sized by magnitude. The earliest events occur below well 16A(78)-32 while later events occur along a linear path further to the east when viewed from the south.

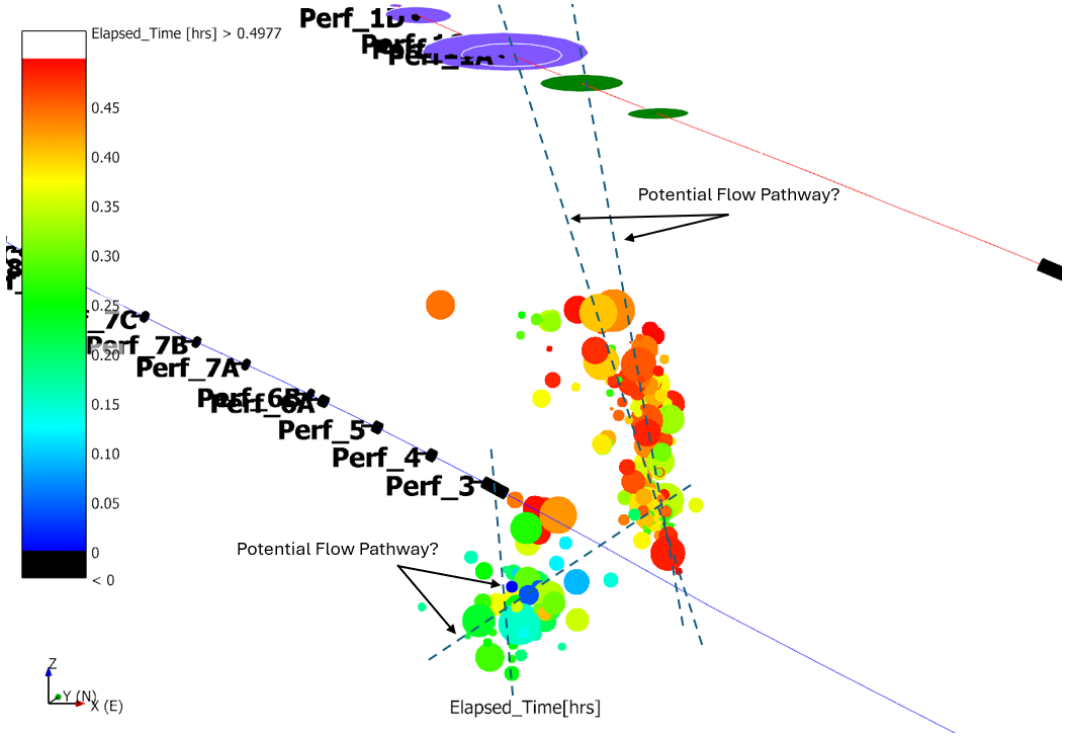

Figure 7: Microseismic points recorded during the first 30 minutes of the stimulation of Stage 3 in well 16A(78)-32 suggest two or more fractures may be creating flow pathways between the wells (MEQ data from Dyer et al, 2023).

The first step in the process to define discrete fractures responsible for the flow starting from the perforations at well 16A(78)-32 Stage 3 and reaching the frac hit locations on 16B(78)-32 is to examine the well logs of 16A(78)-32 at the Stage 3 perforation depth interval to see if there is evidence for a pre-existing natural fracture with a geometry that is consistent with the recorded microseismicity. The perforation interval is between 10,120 ft and 10,140 ft MD KB on well 16A(78)-32. While the original Schlumberger FMI log fracture interpretation includes one fracture intersecting the well in this depth, its orientation does not align with very many of the MEQ points (Gilmour et al, 2021). A later FMI fracture interpretation by Handwerger includes several fractures in this depth interval, including one which aligns very well with the microseismic data (Handwerger, 2024). Figure 8 shows the FMI log with the location of the fracture outlined in purple. This is a vertical fracture striking NNE. A fracture intersecting the well at this depth and orientation intersects both the earliest MEQ points below the well and the early MEQ points trending towards the frac hit locations on well 16B(78)-32 (Figure 9). This fracture is included in the DFN with the full name "v1_023A_NF_PP_16AStage3FMI16AH_164ft". The size of the fracture was set to be 164 ft which is large enough to intersect the recorded MEQ points that align with the orientation, but is not extended further as there was not an obvious intersection point suggested by the log data on well 16B(78)-32.

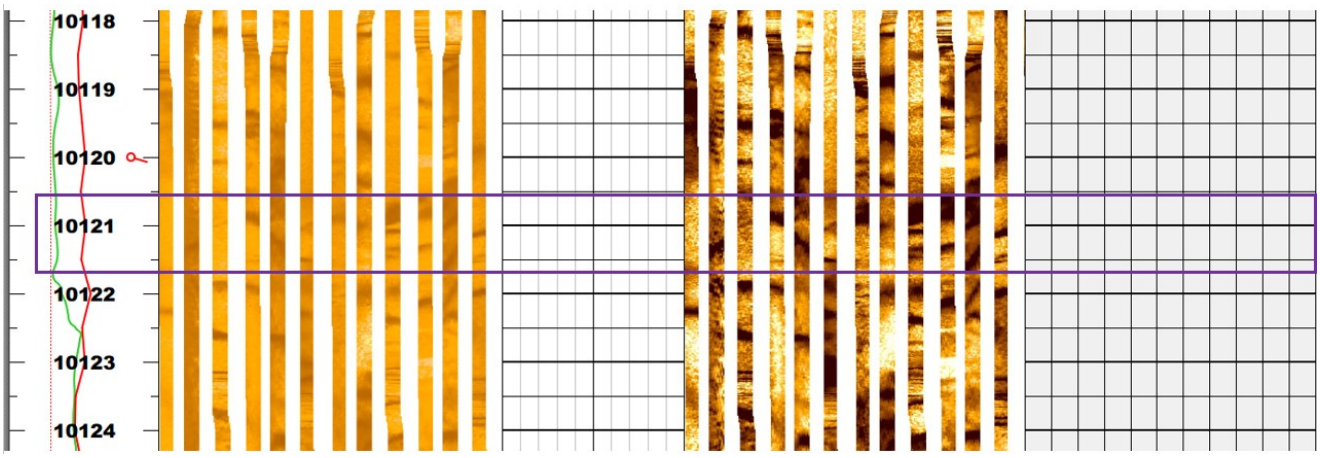

Figure 8: FMI log image showing the location of a Handwerger interpreted fracture in the Stage 3 perforation interval for well 16A(78)-32 (image from Gilmour et al., 2021).

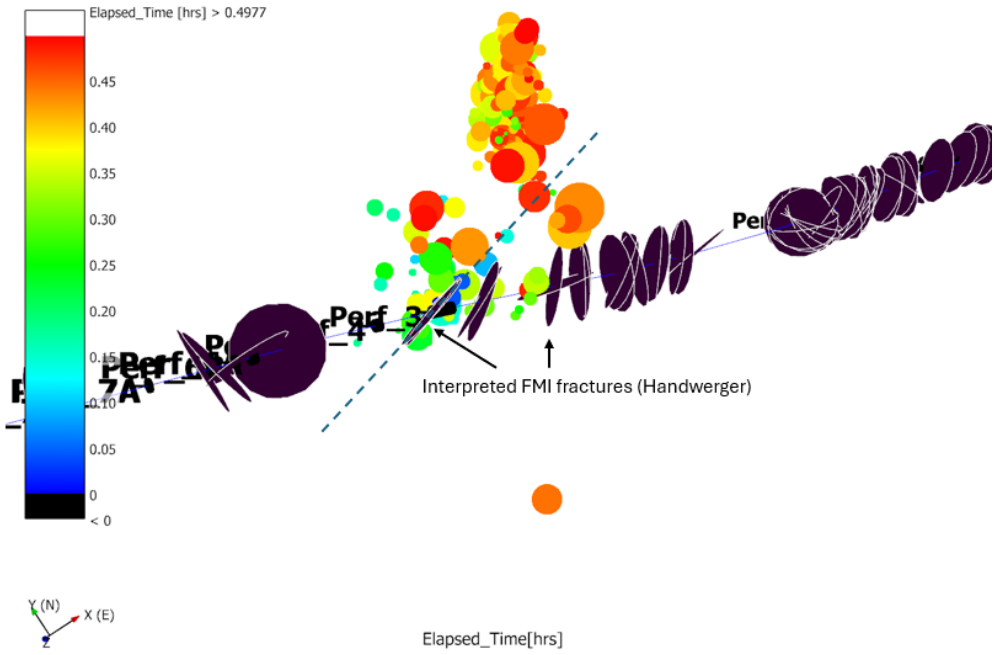

Figure 9: Handwerger interpreted FMI fractures along the borehole of well 16A(78)-32 (black discs show orientations). Microseismic point locations recorded during the first 30 minutes of stimulation of Stage 3 shown in color.

A second fracture was added to the flow pathway to match the alignment of the MEQ points between the wells. This fracture is labeled "v1_024A_NF_PP_16AStage3MSD_324ft" (short name 024A) and was given a size large enough to intersect both well 16A(78)-32 and well 16B(78)-32 after inspecting the log data at those intersection points. Figure 10 shows the thermal neutron porosity log for well 16A(78)-32 with the intersection depth of 024A marked with the dashed black line (Gilmour et al., 2021). The log figures are colored using the results of the cluster analysis performed using both sonic and spectral log data. Different colors highlight different combined rock properties for a range of k-means cluster values (see Finnila and Jones, 2022, for details on the cluster analysis process). The small peak in the porosity along with the change in cluster analysis rock type categorization (color change apparent for k-values 3-8) show some evidence for a fracture intersection point here.

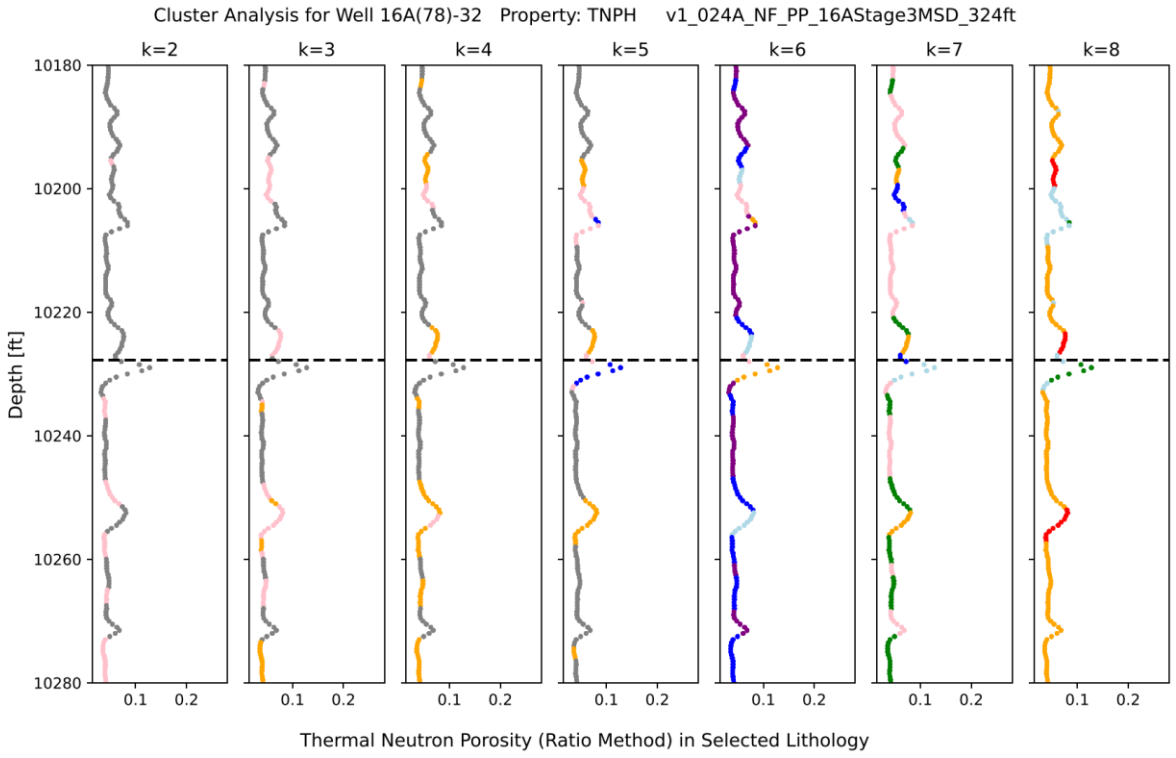

Figure 10: Cluster analysis results for well 16A(78)-32 at k values between 2 and 8 showing the thermal neutron porosity measurements surrounding the intersection point of fracture v1_024A_NF_PP_16AStage3MSD_324ft (dotted line).

The intersection of 024A with well 16B(78)-32 occurs at a depth where core was collected and coincides with a fracture orientation interpreted from the FMI log (Figure 11). While the interpreted fracture orientation at that depth matches that expected from fitting a planar feature to the MEQ points, the wide-aperture, infilled vein just a couple of feet above it may be a better candidate (Figure 12). The core was not oriented when collected and later analysis has adjusted both the assumed core depth and orientation (Jones et al., 2025).

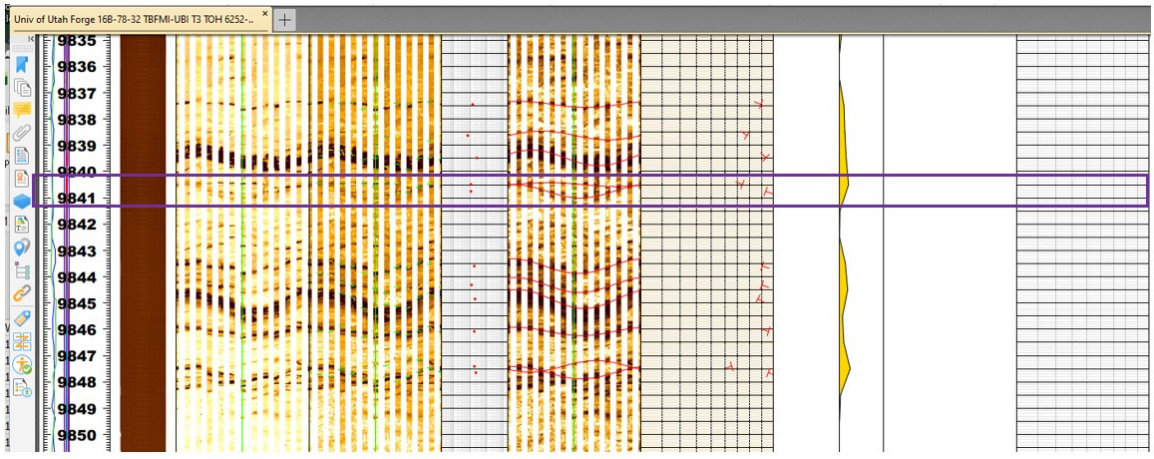

Figure 11: Interpreted FMI log for 16B(78)-32 at the intersection depth with fracture v1_024A_NF_PP_16AStage3MSD_324ft outlined in purple (image from May and Jones, 2023).

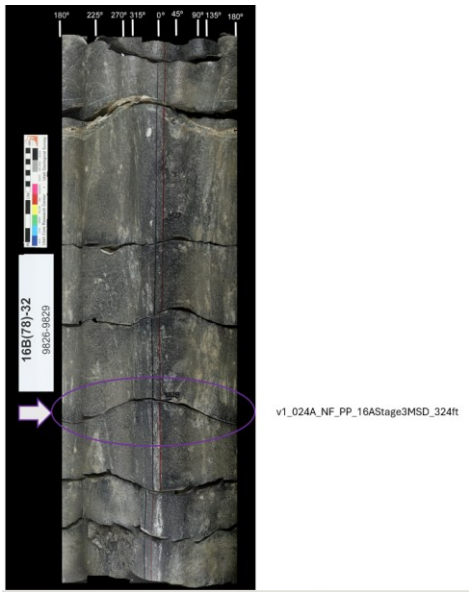

Figure 12: Core sample from well 16B(78)-32 showing fracture matching DFN fracture v1_024A_NF_PP_16AStage3MSD_324ft. Core photo from Jones (2025). Note that location of core fracture has been shifted 13.1 ft from this photo label based on analysis by Jones et al. (2025) so the fracture intersection depth on 16B(78)-32 is assumed to be 9841.15 ft MD KB.

Figure 13 shows the proximity of fracture 024A with frac hit locations on well 16B(78)-32. While the log data for cohesion, friction angle, or gamma ray do not show evidence of a significant pre-exiting feature, the location is very near a frac hit evident from the fiber optic data (location is labeled CWS3 in the figure). Log data is from May and Jones, 2023.

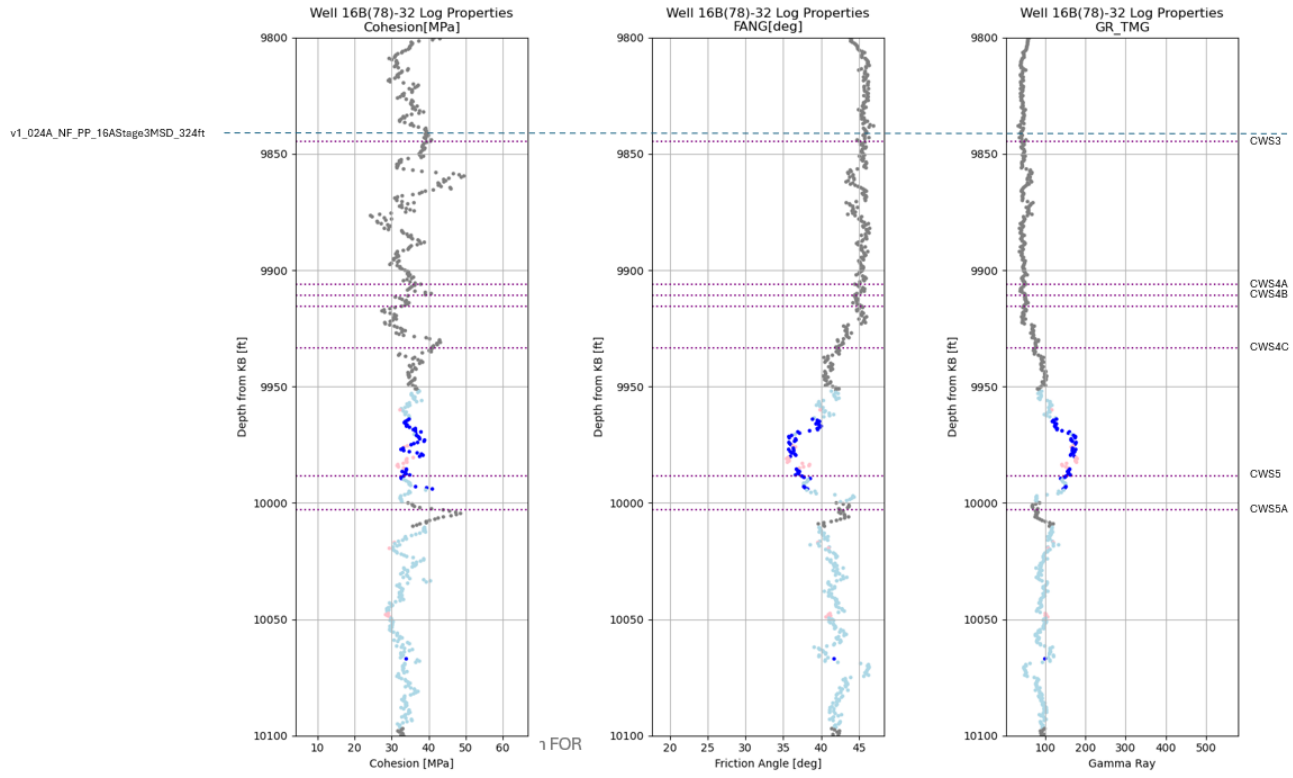

Figure 13: Correlation of the DFN fracture, v1_024A_NF_PP_16AStage3MSD_324ft (blue dotted lines), with frac hit locations and sonic log data on well 16B(78)-32. Colors show the k-means clustering results (k=6) of the analysis performed on the sonic log data to highlight differing rock types. Frac hit identifiers are shown on the right side of the figure with brown and purple dotted lines indicating depths.

The preceding workflow used fractures 023A and 024A as examples. A similar process was followed for all the stimulation stages of well 16A(78)-32 and documentation of that work can be found on the GDR release (Finnila, 2026).

4. DFN CORRELATION WITH DATA SOURCES

While it is useful to see how each DFN fracture has been identified by utilizing the various data sources, it is also instructive to review the full set of DFN fractures in relation to each data set. This exercise can reveal both where expected support is lacking for individual fractures as well as where fractures may have been missed. Figures covering the full suite of data sources are included in the GDR release (Finnila, 2026). The following subsections on the different data sources highlight the different views available.

4.1 Microearthquake catalogs

While the DFN update was informed by many different data sources, the updated microseismic catalogs from both the surface nodal array and deep geophones were especially valuable for locating flow pathways away from well control and determining fracture sizes (Dyer et al, 2023; Niemz et al., 2024). Figure 14 shows an example of a fracture in the DFN that shows close alignment with the microseismic points recorded by the surface nodal array. Looking down on the edge of the almost vertical fracture makes it appear as a line in the figure. This particular fracture, v1_115A_NF_NP_16AStage9FMI16BF2_1193ft, is also supported by the DAS microseismic reflecting imaging analysis (see west-dipping fault labeled “F2” in Ma et al., 2026).

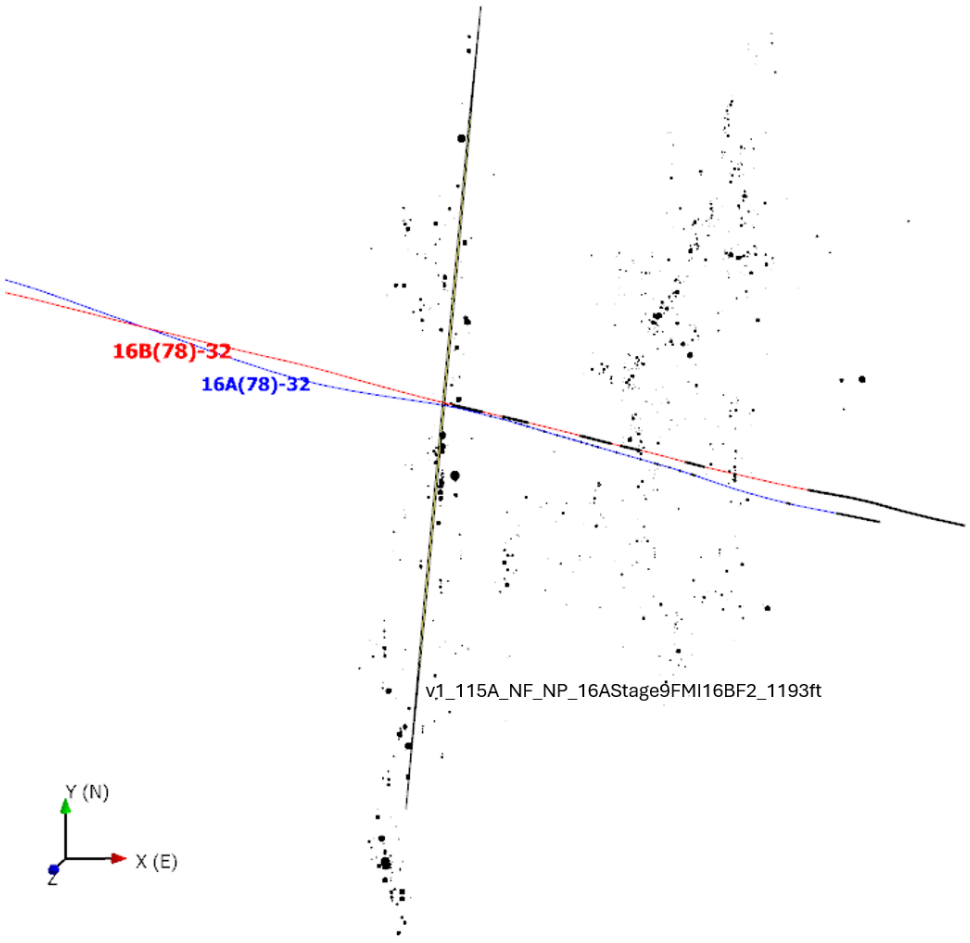

Figure 14: Top-down view of Niemz et al. (2024) microseismic data with one of the DFN fractures Microseismic points sizes are scaled by magnitude. Open hole and stimulation stages are shown in black on well 16A(78)-32 and 16B(78)-32 boreholes.

4.2 FMI and UBI logs

An FMI log (Formation MicroImager log) provides a high-resolution electrical image of a borehole wall. Images are usually generated using two color normalization methods: static logs use a fixed color scale for the entire interval to show overall facies/lithology contrasts, while dynamic logs use a sliding window (e.g., 2m) to enhance local contrast, making them ideal for spotting fine details like fractures and bedding.

4.2.1 Static FMI

Color changes in static FMI logs can indicate where significant fractures, fault zones, or lithology boundaries intersect a wellbore. Rock altered by fluid flow often appears darker in the static FMI image and different lithologies may have appreciably different electric resistivity values. Figure 15 shows a section of the FMI and UBI logs for well 16B(78)-32 showing locations of intersections with the DFN fractures. From the static log shown in this figure, the two DFN fractures v1_115A_NF_NP_16AStage9FMI16BF2_1193ft and v1_103B_NF_NP_16AStage8MSSF2_1193ft align with the darkest color with significant color shading around this feature extending approximately ten feet, indicating a possibly significant fault zone.

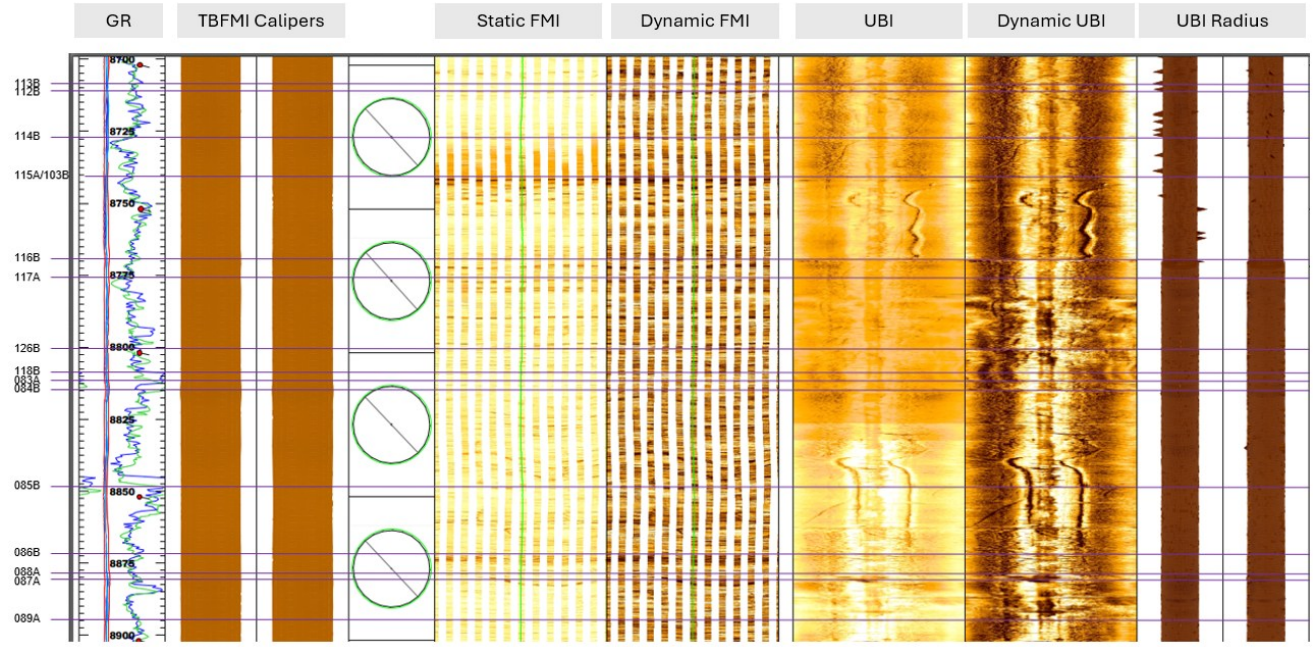

Figure 15: Section of FMI and UBI logs for well 16B(78)-32 showing locations of intersections with DFN fractures (purple lines). Short fracture names included as labels on the left side of figure. Log image from file "Univ of Utah Forge 16B-78-32 TBFMI-UBI Trip3 TOH 6252-10914 5in.pdf" included in GDR release May and Jones (2023).

4.2.2 Interpreted FMI and UBI logs

Dynamic FMI logs and UBI logs are often used to identify fractures intersecting the wellbore. These fracture interpretations can include estimates of fracture orientation and aperture. Well 16A(78)-32 has two FMI log fracture interpretations while well 16B(78)-32 has both an FMI interpretation and a UBI interpretation (Gilmour et al., 2021; Handwerger, 2024; May and Jones, 2023). Interpreted FMI logs are also available for wells 58-32, 56-32, and 78B-32 (Nash and Moore, 2018; Bristol et al., 2021; McLennan, 2021). Figure 16 shows a section of the interpreted FMI and UBI logs for well 16B(78)-32 showing the location DFN fracture v1_115A_NF_NP_16AStage9FMI16BF2_1193ft.

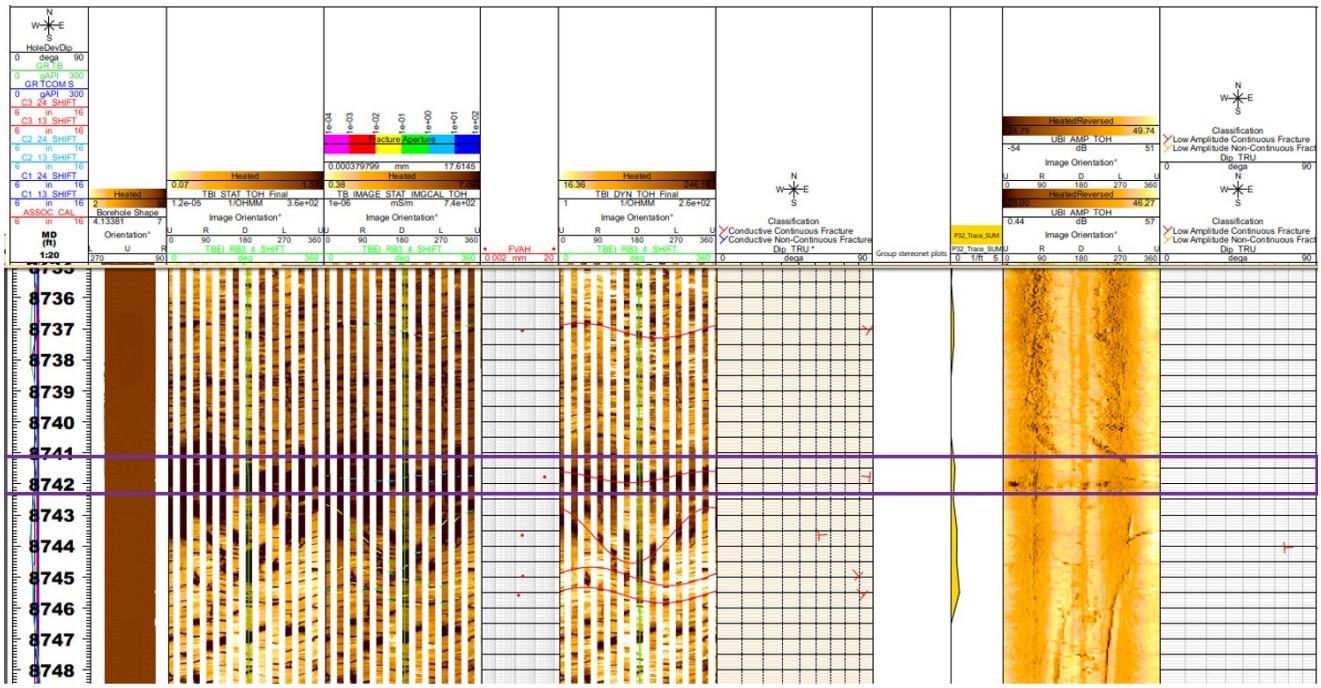

Figure 16: Section of interpreted FMI and UBI logs for well 16B(78)-32 showing location of intersection with DFN fracture v1_115A_NF_NP_16AStage9FMI16BF2_1193ft (outlined by purple lines). The orientation of this DFN fracture was copied from the interpreted vertical conductive continuous fracture at the depth of 8741.78 ft MD KB (see red "T" symbol showing strike and dip). Log image from file "Univ of Utah Forge 16B-78-32 TBFMI-UBI T3 TOH 6252-10914 60in.pdf" included in GDR release May and Jones (2023).

4.3 K-means cluster analysis of log data

Performing a k-means cluster analysis on well log data is a quick way to classify the intercepted rock into groups sharing similar measured properties. These properties might describe intact lithology or the mechanical state of the rock, such as fractured vs unfractured. Care must be taken when combining data from different logs to confirm the assigned depths of measurements are consistent. For instance, the cluster analysis work on well 16A(78)-32 for use in developing the DFN included both a spectral log and acoustic log where an initial comparison of the gamma logs included in both showed some mismatch. Before performing the cluster analysis, the assigned depths for the spectral log data were adjusted to improve the gamma ray correlation. Cluster analyses were done for all five deep wells and figures created to show where DFN fractures intersect the well boreholes as seen in Figure 17. In these figures, group color assignments are arbitrary and do not indicate any identified lithology or mechanical state. All figures are available on the GDR (Finnila, 2026).

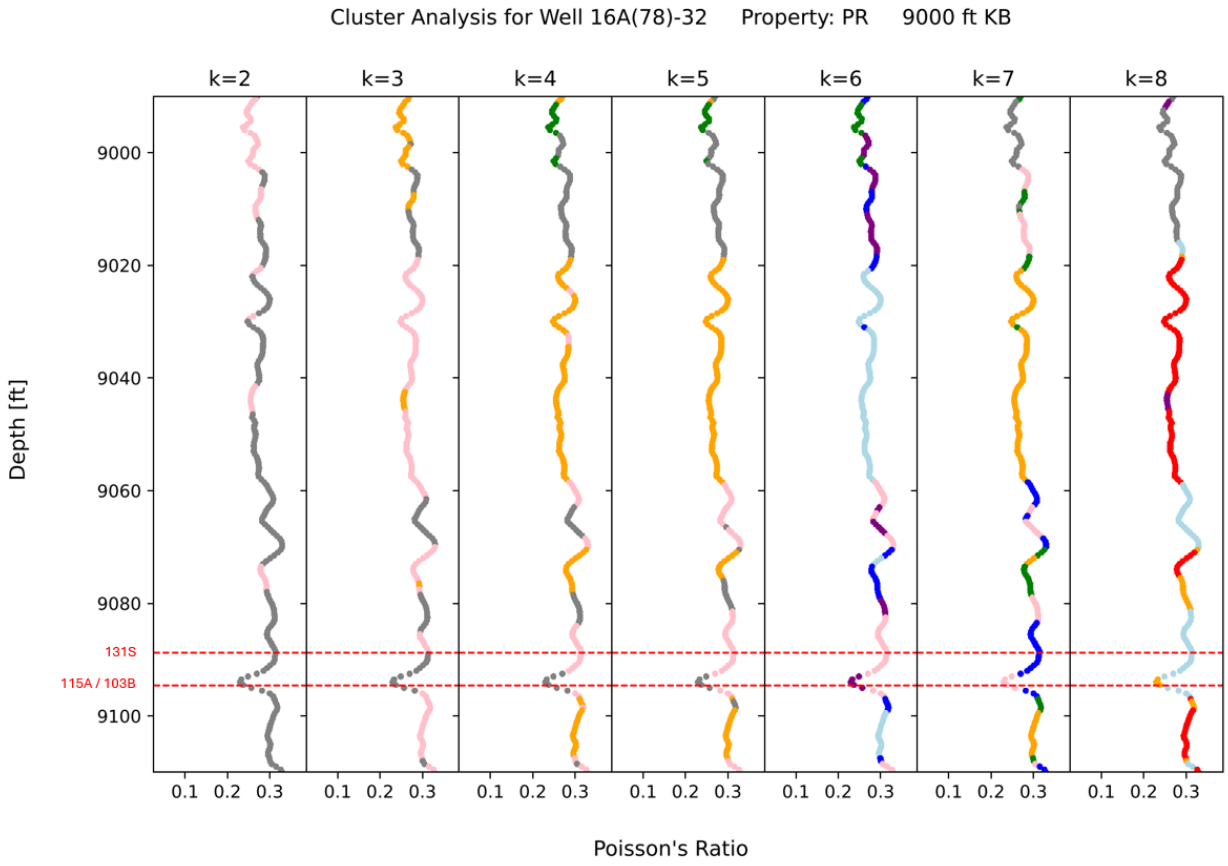

Figure 17: Cluster analysis results for well 16A(78)-32 at k values between 2 and 8 showing Poisson's ratio acoustic log values at depths between 9000 ft and 9100 ft along with the intersection points of DFN fractures (dotted red lines). Poisson's ratio log data from Gilmour et al., 2021.

4.4 Frac hit locations

The DFN update used interpreted frac hit locations on 16B(78)-32 to aid in the identification of active flow pathways following stimulation of 16A(78)-32. These locations were selected by selecting peaks from the strain change rates calculated from the cross-well Rayleigh Frequency Shift Distributed Strain Sensing (RFS DSS) data collected from the installed fiber in well 16B(78)-32 during the stimulation of well 16A(78)-32 in 2024 (Jurick et al., 2025). Locations showing peak values at or above 0.15 microstrain units were included and given a unique identifier (Table 2). While the 3D geometry of the DFN fractures is complex, a 2D trace plane vertically aligned with the well laterals showing their approximate intersections with this feature can be used to examine the alignment between DFN and frac hit locations (Figure 18). A spreadsheet of exact intersection well depths of the DFN is provided in the GDR release of the DFN (Finnila, 2026).

Table 2: Frac hit locations used for DFN development.

FDI Identifier	Measured Depth (ft) in reference Kelly Bushing	Strain change rate (microstrain)		FDI Identifier	Measured Depth (ft) in reference Kelly Bushing	Strain change rate (microstrain)
CWS0A	8617.63	0.41		CWS2G	9036.16	0.15
CWS0B	8646.62	0.16		H10	9056.15	0.33
CWS0C	8660.61	0.18		CWS2H	9244.76	0.17
CWS0D	8680.94	0.21		H11	9267.09	0.44
CWS0E	8692.27	0.15		CWS2J	9272.75	0.16
CWS0F	8701.93	0.22		H12	9346.06	0.25
CWS1	8711.26	0.38		H14	9435.37	0.72
CWS1A	8728.59	0.22		H15	9449.03	0.42
CWS1B	8741.92	0.18		H16	9466.02	0.25
CWS1C	8757.58	0.22		H17	9477.35	0.15
CWS2	8769.58	0.28		H19	9525.67	0.17
H1	8776.27	0.26		H20	9554.33	0.18
S9A	8806.90	0.25		H21	9576.65	0.15
S9B	8814.23	0.41		H23	9643.64	0.15
H2	8817.89	0.38		CWS2K	9662.30	0.17
S9C	8831.90	0.36		H24	9674.63	0.17
H3	8836.56	0.43		CWS2L	9689.62	0.19
S8A	8848.55	0.58		H25	9693.95	0.45
H4	8870.54	1.00		S6A	9708.95	0.17
CWS2A	8875.21	0.45		CWS2M	9720.61	0.39
H5	8880.88	0.67		CWS2N	9729.94	0.17
S9D	8889.21	0.32		S3RA	9746.94	0.54
H6	8894.87	0.45		S3RB	9759.27	0.62
S9E	8905.20	0.24		H26	9763.26	0.28
S10A	8910.20	0.24		H27	9770.93	1.00
S8B	8916.20	0.41		H28	9780.59	0.30
S9F	8921.53	0.23		S3RC	9792.25	0.28
CWS2B	8926.86	0.18		CWS3	9844.57	0.29
CWS2C	8941.52	0.16		CWS4A	9906.22	0.26
H7	8960.52	0.32		CWS4B	9910.88	0.25
CWS2D	8967.85	0.17		CWS4C	9915.55	0.16
CWS2E	8992.17	0.19		CWS4D	9933.54	0.15
H8	9000.50	0.36		CWS5	9988.53	0.18
CWS2F	9006.84	0.20		CWS5A	10002.86	0.15
H9	9028.83	0.16				

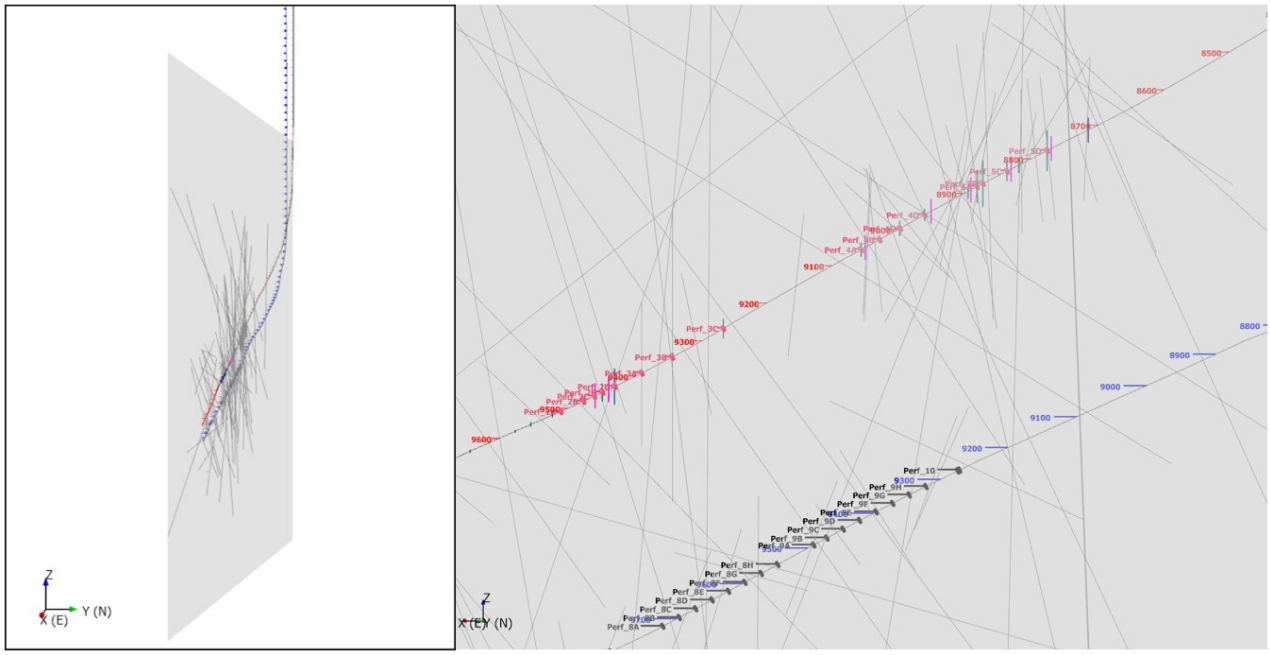

Figure 18: DFN fracture traces (grey lines) on a vertical plane aligned with wells 16A(78)-32 and 16B(78)-32. Pink and green vertical bars on 16B(78)-32 show locations of interpreted frac hits. Note that fracture locations are somewhat approximate as the vertical trace plane cannot align exactly with the entire length of the well trajectories.

Another figure showing combined cluster analysis results and the location of frac hits along with the DFN fracture intersection depths is shown in Figure 19. Many DFN fractures were included specifically to intersect frac hit locations in 16B(78)-32 that showed the most fiber strain.

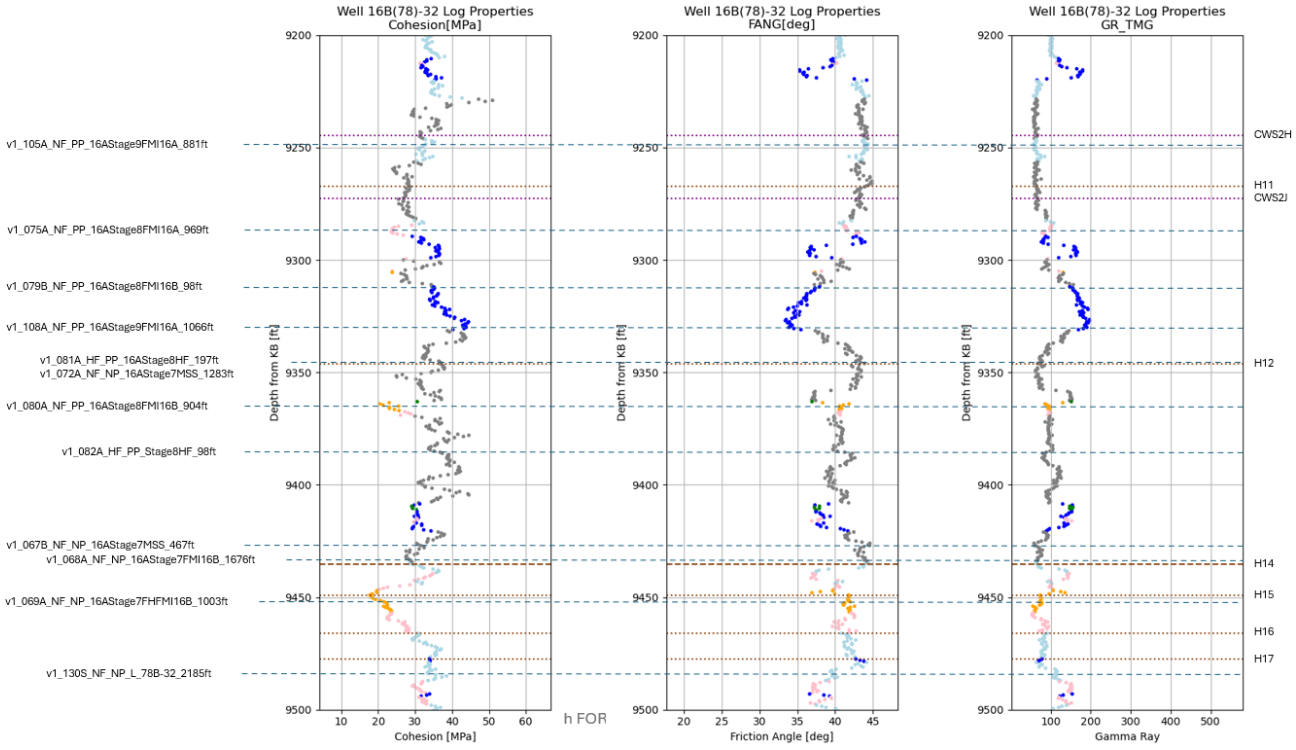

Figure 19: Correlation of the DFN with frac hit locations and sonic log data on well 16B(78)-32. Colors show the k-means clustering results (k=6) of the analysis performed on the sonic log data to highlight differing rock types. Fracture ids are shown on the left side of the figure (blue dotted lines) while frac hit identifiers are shown on the right side (brown and purple dotted lines). Log data is from May and Jones, 2023.

4.5 Core samples

Two of the DFN fractures can be mapped to features seen in core: v1_024A_NF_PP_16AStage3MSD_324ft (Figure 12) and v1_066A_NF_NP_16AStage7MSS_1430ft. These cores were collected from well 16B(78)-32 and are in the "Stimulation 3" core collection. Both match smaller identified FMI fractures located just below more prominent thick veins with apertures of up to 1 cm that contain open cavities lined with euhedral crystals (Jones et al., 2025). Both fractures were identified primarily though fitting planar features through the microseismic data sets. Getting better consistency between the microseismic data, large aperture FMI fractures, and core would be desirable in a future DFN update.

Interestingly, locations where the DFN fractures intersect targeted cored intervals, but no core was recovered may provide indirect positive evidence of the existence of a fracture at that location as a highly fractured zone is harder to retrieve while coring. This seems to be the case for fractures v1_017B_NF_NP_16AStage2MSD_376ft ("Stimulation 1" core collection) and v1_018B_NF_NP_16AStage2MSD_440ft ("Stimulation 2" core collection). Both fractures were identified primarily though fitting planar features through the microseismic data collected at depth.

4.6 Data Source Documentation

Two comprehensive resources for viewing the relationships between the DFN and the various data sources are available on the GDR. The DFN fractures and some of the data sets are loaded onto online viewers that may be rotated in 3D from a web browser (Jones and Finnila, 2026). It is especially helpful to rotate the views in order to visualize how individual fractures align with the microseismic data. These views are accompanied by two tables which document evidence from various data sets supporting individual fractures. Figure 20 shows a portion of the summary evidence table and Figure 21 shows a portion of the MEQ detail table where the MEQ data sets are divided by stimulation stage. Note that the full tables include rows for all the 133 discrete fractures.

Utah FORGE 2025v1 DFN Fracture Name	16A(78)-32 Intersection Depth [MD KB ft]	16B(78)-32 Intersection Depth [MD KB ft]	16A(78)-32 Static FMI	16A(78)-32 Handwerger Interpreted FMI	16B(78)-32 Static FMI	16B(78)-32 Interpreted FMI/UBI	Dyer et al., 2024 Microseismic	Niemz et al., 2024 Microseismic	16B(78)-32 2024 DSS Frac Hits
v1_001A_NF_NP_16AStage1MSD_459ft	10826.5	N/A	Y	n	N/A	N/A	y	n	N/A
v1_001S_NF_NP_16AStage1MSD_800ft	10829.9	10678.3	Y	n	y	n	y	n	N/A
v1_002A_NF_NP_16AStage1MSD_460ft	N/A	N/A	N/A	N/A	N/A	N/A	Y	n	N/A
v1_002S_NF_NP_16AStage1MSD_2559ft	N/A	10015.3	N/A	N/A	n	n	y	y	n
v1_003A_NF_NP_16AStage1FMI16B_604ft	10520.7	10313.6	Y	n	y	Y	Y	Y	N/A
v1_004A_NF_NP_16AStage1MSD_1185ft	10579.9	10499.4	y	y	y	n	y	y	N/A
v1_005B_NF_NP_16AStage1MSD_600ft	10558.6	10409.8	Y	n	y	y	Y	n	N/A
v1_006B_NF_NP_16AStage1MSD_506ft	10773.0	N/A	n	n	N/A	N/A	y	n	N/A
v1_007B_NF_NP_16AStage1MDS_115ft	N/A	N/A	N/A	N/A	N/A	N/A	y	n	N/A
v1_008B_NF_NP_16AStage1MDS_168ft	N/A	N/A	N/A	N/A	N/A	N/A	y	n	N/A
v1_009B_NF_NP_16AStage1MSD_392ft	N/A	N/A	N/A	N/A	N/A	N/A	Y	n	N/A
v1_010B_NF_NP_16AStage1MSD_459ft	10523.3	N/A	Y	n	N/A	N/A	y	n	N/A
v1_011B_NF_NP_16AStage1MSD_305ft	N/A	N/A	N/A	N/A	N/A	N/A	y	n	N/A
v1_012B_NF_NP_16AStage1MSD_460ft	N/A	N/A	N/A	N/A	N/A	N/A	y	n	N/A
v1_013B_NF_NP_16AStage1MSD_305ft	N/A	N/A	N/A	N/A	N/A	N/A	y	n	N/A
v1_014B_NF_NP_16AStage1MSD_451ft	N/A	10058.9	N/A	N/A	n	n	y	n	n
v1_015B_NF_NP_16AStage1MSD_793ft	10855.7	N/A	y	n	N/A	N/A	y	y	N/A
v1_016B_NF_NP_16AStage2MSD_118ft	N/A	N/A	N/A	N/A	N/A	N/A	y		
v1_017B_NF_NP_16AStage2MSD_376ft	10277.4	10457.7	n	n	y	n	Y		
v1_018B_NF_NP_16AStage2MSD_440ft	10302.4	10280.2	y	n	y	y	Y		
v1_019B_NF_NP_16AStage2MSD_413ft	N/A	9987.5	N/A	N/A	n	n	y		
v1_020B_NF_NP_16AStage2MSD_451ft	N/A	10378.9	N/A	N/A	n	y	y		

N/A	no fracture intersection
n	no evidence
y	weak evidence
Y	strong evidence

Figure 20: Portion of summary table included in the GDR release to catalog which data sets show evidence for individual DFN fractures (Jones and Finnila, 2026).

	16A(78)-32 MEQ												16B(78)-32 MEQ		
Utah FORGE 2025v1 DFN Fracture Name	Stage 1	Stage 2	Stage 3	Stage 3R	Stage 4	Stage 5	Stage 6A	Stage 6B	Stage 7	Stage 8	Stage 9	Stage 10	Stage 1	Stage 2	Stage 3
v1_001A_NF_NP_16AStage1MSD_459ft	y	n	n	n	n	n	n	n	n	n	n	n	n	n	n
v1_001S_NF_NP_16AStage1MSD_800ft	y	n	n	n	n	n	n	n	n	n	n	n	n	n	n
v1_002A_NF_NP_16AStage1MSD_460ft	y	Y	n	n	n	n	n	n	n	n	n	n	n	n	n
v1_002S_NF_NP_16AStage1MSD_2559ft	y	y	y	y	y	y	y	y	y	y	y	y	n	n	n
v1_003A_NF_NP_16AStage1FMI16B_604ft	y	Y	y	n	n	n	n	n	n	n	n	n	n	n	Y
v1_004A_NF_NP_16AStage1MSD_1185ft	y	y	n	n	n	y	n	y	y	y	y	y	n	n	n
v1_005B_NF_NP_16AStage1MSD_600ft	Y	y	n	n	n	n	n	n	n	n	n	n	n	n	n
v1_006B_NF_NP_16AStage1MSD_506ft	y	y	n	n	n	n	n	n	n	n	n	n	n	n	n
v1_007B_NF_NP_16AStage1MDS_115ft	y	n	n	n	n	n	n	n	n	n	n	n	n	n	n
v1_008B_NF_NP_16AStage1MDS_168ft	y	y	n	n	n	n	n	n	n	n	n	n	n	n	n
v1_009B_NF_NP_16AStage1MSD_392ft	Y	y	n	n	n	n	n	n	n	n	n	n	n	n	n
v1_010B_NF_NP_16AStage1MSD_459ft	y	y	n	n	n	n	n	n	n	n	n	n	n	n	n
v1_011B_NF_NP_16AStage1MSD_305ft	y	n	n	n	n	n	n	n	n	n	n	n	n	n	n
v1_012B_NF_NP_16AStage1MSD_460ft	y	y	n	n	n	n	n	n	n	n	n	n	n	n	n
v1_013B_NF_NP_16AStage1MSD_305ft	y	n	y	n	n	n	n	n	n	n	n	n	n	n	n
v1_014B_NF_NP_16AStage1MSD_451ft	y	y	n	n	n	n	n	n							
v1_015B_NF_NP_16AStage1MSD_793ft	y	y	y	y	y	y	n	n							
v1_016B_NF_NP_16AStage2MSD_118ft	y	y	n	n	n	n	n	n							
v1_017B_NF_NP_16AStage2MSD_376ft	y	Y	y	n	y	n	n	n							
v1_018B_NF_NP_16AStage2MSD_440ft	y	Y	y	n	n	n	n	n							
v1_019B_NF_NP_16AStage2MSD_413ft	y	y	n	n	n	n	n	n							
v1_020B_NF_NP_16AStage2MSD_451ft	y	y	n	n	n	n	n	n							

	fracture and MEQ evidence in same 16A(78)-32 stage
	fracture and MEQ evidence not in same 16A(78)-32 stage
	fracture aligns with 16B(78)-32 stage MEQ
n	no evidence
y	weak evidence - lighter color
Y	strong evidence - darker color

Figure 21: Portion of detail table included in the GDR release to catalog which stimulation stage MEQ data sets show evidence for individual DFN fractures (Jones and Finnila, 2026).

The second main source of documentation of the relationships between the DFN and the various data sources is the recent release to the GDR of the thousands of figures generated while developing the DFN. Examples of these figures have been used in this paper. The figures are organized both by individual fracture as well as by each data source and are made available in pdf file collections (Finnila, 2026).

5. CONCLUSION

The Utah FORGE v1 DFN is available for use by modelers interested in simulation flow between wells 16A(78)-32 and 16B(78)-32. By excluding discrete fractures designated as being hydraulic fractures (presumably ones created during previous stimulation activities), modelers wanting to simulate the stimulation activities already performed on the wells may find this DFN useful as well. Subsets of the discrete fractures can be used to provide simpler models for specific purposes.

Some key limitations of the DFN include the following:

- The DFN only describes the geometry of the flow pathways, not hydraulic properties such as aperture, permeability, or compressibility which may be variable within an individual fracture plane.
- Fracture sizes are estimated based on available MEQ intersections, evidence of intersection with one or more of the five deep wells in the reservoir based on log data, estimates of aperture from FMI logs, or magnitudes of frac hits on 16B(78)-32. Modelers are encouraged to adjust fracture sizes as required for their particular simulation objectives.
- It is geologically reasonable to assume that some of these fractures are truncated by others which is not represented in the current DFN.
- The DFN was developed primarily to support the simulation of flow between 16A(78)-32 and 16B (78)-32. Other significant fractures may be discovered with more attention to the data sets for 58-32, 78B-32, and 56-32 as well as regions on 16A(78)-32 and 16B(78)-32 outside of the current modeling region.

During the development of the DFN, there were a few observations made which may direct future work:

- Flow paths generally follow pre-existing natural fractures as can be seen in the following counts:
  - Natural fractures (126)
  - Hydraulic fractures (5)
- MEQ locations often occur in lines which are assumed to form at the intersections of two fracture planes. Does this mean flow is generally restricted to these linear, as opposed to planar, flow pathways? If so, this may result in a much-reduced fracture area for thermal exchange in the producing reservoir.
- Static FMI is useful in 16A(78)-32 to highlight potential alteration zones while detailed fracture interpretations seemed problematic due to poor alignment between pad images.
- MEQ locations from both the nodal surface arrays and the geophones at depth were very consistent with other data sets for locating fractures and vital for sizing their extents.
- Having accurate well locations and trajectories as well as accurate depth control in the log data is critical for being able to identify data alignment across different data sources.
- MEQ locations near the stimulation stages can be very useful for identifying corresponding image log fracture picks which may be involved in initial flow pathways.
- Performing k-means cluster analysis of log data seems to be a fast and effective way to combine multiple log properties and highlight potential fault zones or lithologic boundaries.

The next iteration of the Utah FORGE DFN will be developed once new data sets are available from planned activities in the coming year which may include longer-term circulation testing, additional stimulation activities, and drilling a new well with the acquisition of more log suites.

ACKNOWLEDGEMENTS

Funding for this work was provided by the U.S. DOE under grant DE-EE0007080 “Enhanced Geothermal System Concept Testing and Development at the Milford City, Utah FORGE Site.”

REFERENCES

Bristol, J., Caldwell, S., Welch, V., Stroud, P., Williams-Mieding, B., Broderick, P., Schepflin, A., Van Gaal, M., Mozena, T., Rivas, E., Nash, G., McLennan, J., & Handwerger, D. (2021). Utah FORGE: Well 56-32 Drilling Data and Logs. [Data set]. Geothermal Data Repository. Energy and Geoscience Institute at the University of Utah. https://doi.org/10.15121/1777170

Dyer, B., Karvounis, D., Bethmann, F. (2023). Microseismic event catalogues from the well 16A(78)-32 stimulation in April, 2022 in Utah FORGE., ISC Seismological Dataset Repository, https://doi.org/10.31905/52CC4QZB

Finnila, A. and Jones, C.: Rapid Rock Type Categorization at Utah FORGE from Sonic Logs using K-Means Clustering, GRC Transactions, Vol. 46, (2022)

Finnila, A., & Jones, C. (2024a). Updated Reference Discrete Fracture Network Model at Utah FORGE. Proceedings of the 49th Workshop on Geothermal Reservoir Engineering, Stanford University, Stanford, CA

Finnila, A., & Jones, C. (2024b). Utah FORGE: 2024 Discrete Fracture Network Model Data . [Data set]. Geothermal Data Repository. Energy and Geoscience Institute at the University of Utah. https://doi.org/10.15121/2440870

Finnila, A. (2025). Utah FORGE: Updated Discrete Fracture Network Model - 2025. [Data set]. Geothermal Data Repository. WSP. https://gdr.openei.org/submissions/1750

Finnila, A. (2026). Utah FORGE: Updated Discrete Fracture Network Model – 2025. DFN Development Notes [Data set]. Geothermal Data Repository. WSP. https://gdr.openei.org/submissions/1750

Gilmour, B., Wooden, J., Pulka, F., Rose, B., Barker, C., & Borchardt, E. (2021). Utah FORGE: Well 16A(78)-32 Logs. [Data set]. Geothermal Data Repository. Energy and Geoscience Institute at the University of Utah. https://doi.org/10.15121/1777912

Handwerger, D. (2024). Utah FORGE: Updated FMI Fracture Log from Well 16A(78)-32. [Data set]. Geothermal Data Repository. Energy and Geoscience Institute at the University of Utah. https://doi.org/10.15121/2339498

Jones, C. (2025). Utah FORGE: Well 16B(78)-32 Drill Core Fracture Analysis Images and Data. https://gdr.openei.org/submissions/1708

Jones, C., McLennan, J., & Moore, J. (2025). Characterization of Drill Core from Stimulated Crystalline Rock Following Hydraulic Fracturing at the Utah FORGE Geothermal Test Site. Proceedings of the 50th Workshop on Geothermal Reservoir Engineering, Stanford University, Stanford, CA

Jones, C., & Finnila, A. (2026). Utah FORGE: Discrete Fracture Network Model 3D Visualization Via the Sequent Central Public Viewer - 2025 V1. [Data set]. Geothermal Data Repository. Energy and Geoscience Institute at the University of Utah. https://gdr.openei.org/submissions/1807

Jurick, D., Khatara, S., & Davidson, E. (2025). Utah FORGE: 16B(78)-32 RFS DSS Strain Change Rate and Selected FDIs During 16A(78)-32 Stimulation. [Data set]. Geothermal Data Repository. Neubrex Energy Services (US), LLC. https://doi.org/10.15121/2531107

Ma, Y., Ajo-Franklin, J., Chamarczuk, M., Zhu, X., Patterson, J., Rodriguez, I. V., et al. (2026). Geothermal reservoir characterization at Utah FORGE using DAS microseismic imaging. Journal of Geophysical Research: Solid Earth, 131, e2025JB032603. https://doi.org/10.1029/2025JB032603

May, D., & Jones, D. (2023). Utah FORGE: Well 16B(78)-32 Logs from Schlumberger Technologies. [Data set]. Geothermal Data Repository. Energy and Geoscience Institute at the University of Utah. https://doi.org/10.15121/2001059

McLennan, J. (2021). Utah FORGE: Well 78B-32 Daily Drilling Reports and Logs. [Data set]. Geothermal Data Repository. Energy and Geoscience Institute at the University of Utah. https://doi.org/10.15121/1814488

Nash, G., & Moore, J. (2018). Utah FORGE: Logs and Data from Deep Well 58-32 (MU-ESW1) . [Data set]. Geothermal Data Repository. Energy and Geoscience Institute at the University of Utah. https://doi.org/10.15121/1452735

Niemz, P., Pankow, K., Isken, M., Whidden, K., McLennan, J., & Moore, J. (2024). Utah FORGE: 2024 Stimulations Microseismic Event Catalog from Seismic Surface Network. [Data set]. Geothermal Data Repository. University of Utah Seismograph Stations. https://gdr.openei.org/submissions/1622